Integrated In-Cylinder / CHT Methodology for the Simulation of the Engine Thermal Field: An Application to High Performance Turbocharged DISI Engines

Giuseppe Cicalese
R&D CFD SRL

Fabio Berni and Stefano Fontanesi
Universita degli Studi di Modena

ABSTRACT

New SI engine generations are characterized by a simultaneous reduction of the engine displacement and an increase of the brake power; such targets are achieved through the adoption of several techniques such as turbocharging, direct fuel injection, variable valve timing and variable port lengths. This design approach, called "downsizing", leads to a marked increase in the thermal loads acting on the engine components, in particular on those facing the combustion chamber. Hence, an accurate evaluation of the thermal field is of primary importance in order to avoid mechanical failures. Moreover, the correct evaluation of the temperature distribution improves the prediction of pointwise abnormal combustion onset.

The paper proposes an evolution of the CFD methodology previously developed by the authors for the prediction of the engine thermal field, which is applied to two different high performance turbocharged DISI engines: the methodology employs both in-cylinder 3D-CFD combustion simulations and CHT (Conjugate Heat Transfer) simulations of the whole engine, inclusive of both the solid components and the coolant circuit. In-cylinder analyses are used as thermal boundary conditions for the CHT simulations, which are in turn a fundamental benchmark to evaluate the accuracy of the combustion heat flux estimation by means of a combination of global engine thermal survey and local temperature measurements.

A preliminary evaluation of some consolidated heat transfer models is carried out to evaluate the accuracy of the predicted gas-to-wall heat fluxes. Then, a modified heat transfer model is proposed, critically motivated and applied to the specific engine conditions under investigations. The proposed model strongly improves the predictive capability of the combined in-cylinder/CHT methodology in terms of both global thermal balance and pointwise temperature distribution for both the investigated engines.

CITATION: Cicalese, G., Berni, F., and Fontanesi, S., "Integrated In-Cylinder / CHT Methodology for the Simulation of the Engine Thermal Field: An Application to High Performance Turbocharged DISI Engines," *SAE Int. J. Engines* 9(1):2016, doi:10.4271/2016-01-0578.

INTRODUCTION

Recent developments in internal combustion engines are strictly guided by fuel consumption reduction and the simultaneous increase of specific brake power.

These targets are achieved by means of different techniques, among which turbocharging, engine downsizing and down-speeding, complex fuel injection strategies, variable valve timing, variable port length [1,2]. These approaches are often jointly adopted and, for more complex configurations, hybridization is also introduced.

If, on one hand, this development pathway is shared between compression and spark ignition engines, on the other hand SI engines are those undergoing the most relevant evolution. For such engines, the increase of the specific power by means of downsizing and

turbocharging has to face with the occurrence of abnormal combustions, which can strongly limit the engine performance [3]. Moreover, the raise of the thermal loads acting on the engine components can reduce their mechanical strength and can deeply reduce the engine reliability because of thermo-mechanical failures. [4]

A correct estimate of the gas-to-wall thermal loads is then fundamental since the early design stages, where CFD and FE tools can be proficiently used to reduce time- and cost-to market. To increase the reliability of such numerical tools, it is of primary importance to accurately define the combustion heat transfer to the engine components. This can be derived from either dedicated experiments or from CFD-1D/3D simulations.

From an experimental point of view, it is not easy to properly isolate the thermal power acting on the components facing the combustion chamber. A direct evaluation of the instantaneous heat flux usually requires the adoption of complex, expensive and intrusive sensors [5,6] which cannot be easily used, for example, to evaluate the behavior of moving parts such as the piston and the valves. Furthermore, such measurements can be performed only in limited portions of the components, and the resulting total thermal power due to combustion has to be extrapolated in both space and time. Indirect methods, instead, are widely used in the automotive industry. They consist of a thermal load calculation by means of a thermal survey of the engine: during the experimental tests, all the thermal contributions are identified (heat to lubricant, heat to coolant, brake power, etc.) and this procedure allows to quantify the power globally acting on the engine components. During such tests, thermocouples can also be placed in the most critical engine locations in order to evaluate pointwise temperature distributions.

Once the heat amount is estimated, it can be used in CFD-CHT and FE tools to calculate the thermal field of the engine: it is split among each component (for example head, liner and piston) thanks to a combination of experimental evidences and user experience. The calculation can be assumed to be successfully performed if the resulting temperatures well match the experimental ones. It should be clear that such an approach relies on several approximations, among which heat flux subdivision between all the components and thermal load distribution, which can be either constant in space or distributed on the basis of physical assumptions and experimental evidences.

Assumptions and uncertainties can be reduced by using 3D-CFD tools to calculate the spatial and temporal evolution of the combustion process: this allows to estimate the amount and pointwise distribution of the thermal loads acting on the engine components. A more accurate representation of the engine thermal field is expected, which may be used for example to evaluate design criticalities leading to abnormal combustions or to thermo-mechanical failures.

The integration between 3D-CFD and FE tools aiming at well capturing the engine thermal field under actual operating conditions has been deeply investigated by the authors and several applications to currently made engines show the benefits of an interaction between the in-cylinder simulation framework and the CHT (i.e. Conjugate Heat Transfer) simulation framework [7,8,9,10]. In such interaction, a fundamental role is played by the capability of the in-cylinder model to accurately estimate the wall heat flux due to combustion. This in turn strongly depends on the formulation of the thermal wall function.

Many research groups tried to develop numerical models able to capture the actual heat flux through the combustion chamber boundaries, among which important contributions can be found in [11,12,13,14]. Two major classes of engine simulation models are available: phenomenological models and the CFD ones. In the former, semi-empirical formulations are used for the heat transfer evaluation. In the latter, a more detailed analysis of the heat transfer mechanisms is possible. Regardless the approach, at the present moment it is nearly impossible to identify a unique thermal wall function formulation suitable for all the engine applications because of the very wide range of engine revving speeds, in-cylinder turbulence levels, engine IMEPs (and therefore loads).

This paper aims at proposing a valid approach for current production high performance DISI engines to be used in in-cylinder simulations in order to properly compute (in both magnitude and distribution) high-load heat fluxes acting on the engine components. Once the thermal load is correctly estimated, the CFD-CHT simulations are capable to well describe the engine thermal field. In the paper, such predictive capability is assessed by means of the comparison against both global engine thermal surveys and experimental temperature measurements for two different engines.

ENGINE OVERVIEW

The investigated engines A and B are currently produced direct injection spark ignition (DISI) turbocharged units, V-shaped 8 cylinder and in line 4 cylinder respectively, and their main characteristics are reported in tables 1 and 2. The first engine is analyzed at two different operating conditions: 5000 rpm WOT (peak torque point) and 7000 rpm WOT (peak power point). The second is investigated just at peak power condition, 5200rpm WOT.

Table 1. Main features of the Engine A

B/S	1.05
Operating Condition1	
Revving Speed	7000 rpm
BMEP	18.33 bar
Operating Condition2	
Revving Speed	5000 rpm
BMEP	24.36 bar

Table 2. Main features of the Engine B

B/S	0.93
Operating Condition	
Revving Speed	5200 rpm
BMEP	22.96 bar

CFD-CHT SIMULATIONS FOR ENGINE THERMAL FIELD CALCULATION

General Guidelines

Internal combustion engine thermal field depends on several cross-linked factors: the point-wise temperature distribution is the result of the heat removal effectiveness of the coolant circuit, the total amount of wall heat flux and its spatial distribution over the engine components. Furthermore, the cooling effect due to the lubricating circuit and to the environment has to be taken into account in addition with the heat due to the frictions between the moving parts. In order to include all these phenomena and to well represent the engine thermal field, the authors developed an integrated in-cylinder / CHT approach [15] that is briefly recalled hereafter.

A preliminary simulation of combustion is performed by imposing a uniform wall temperature on the boundaries facing the combustion chamber. The resulting wall heat fluxes are then averaged over 720 °CA to obtain a cycle average point-wise thermal load distribution without losing important information about the most heated portions of the computational domain.

The heat fluxes are then applied as thermal boundary conditions in a CHT model where the solid components (head, block, gasket, valves, valve seats, valve guides, liners) are simulated together with the coolant circuit in order to properly evaluate both the engine temperature field and the heat removed by the coolant. The adoption of cycle averaged heat fluxes relies on the hypothesis that the thermal inertia of the solid components facing the combustion chamber is too high to be sensible to cycle-resolved thermal loads.

The wall temperatures resulting from this framework are then mapped on the boundaries facing the combustion chamber. The incylinder simulation is then repeated with a point-wise temperature distribution, which deeply influences the heat exchanged through the walls. Again, the obtained wall heat fluxes are time-averaged and they are used to calculate the engine temperature field by means of the CHT model. This data exchange between the different frameworks is required to be performed at least twice in order to meet the convergence in terms of temperatures calculated by the CHT model.

CHT simulations are fundamental to consider the mutual effect between the coolant circuit and the solid regions. The thermal field of the engine components depends on the cooling effectiveness and on the thermal load; the three elements are strictly linked to each other: once the cooling system operating conditions are defined and the thermal load is imposed, the numerical thermal field has to match the experimental one.

CHT Model and Numerical Setup

The computational domain includes the coolant circuit and all the surrounding solid components. Moreover, the valves, the valve seats and the valve guides are added to well capture the heat transfer between the different elements. Each solid component is characterized by its own thermal conductivity and a contact resistance is applied between adjacent region to evaluate temperature discontinuities. A schematic representation of the computational domain is represented in Figure 1.
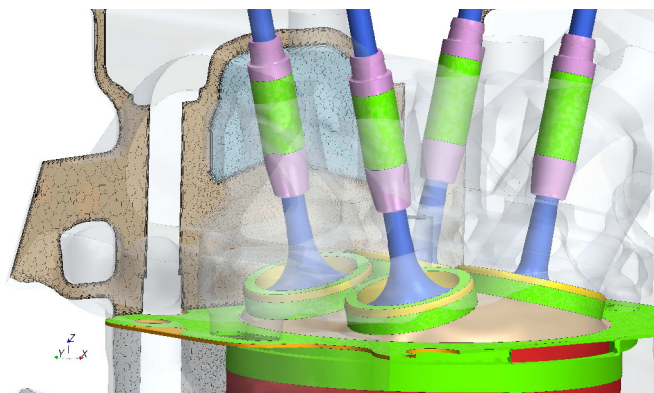

Figure 1. A representation of the computational domain

Pistons are not included in the computational domain, but only the heat exchanged with the cylinder liners is considered, as it will be better explained later in the paper.

Because of the large extent of the computational domain, it is fundamental to limit the number of cells and to speed up the calculation: a polyhedral core mesh and a multi-layer prismatic mesh adjacent to the walls are used to discretize the fluid region, and this approach is suitable for the adopted turbulence model.

On the solid side a multi-layer approach at the walls is chosen to better represent the temperature gradients.

The boundary conditions are time-invariant, i.e. the heat fluxes are not cycle-resolved because of the thermal inertia of the solid components. Furthermore, the moving elements are placed in a fixed position (i.e. valves) or not explicitly included in the computational domain (i.e. pistons). However, a transient solver is needed due to the adoption of a multiphase boiling model to take into account the phase transition in the coolant circuit and the related local increase in heat transfer.

The boundary conditions are derived both from numerical and experimental data: coolant mass flow rates and temperatures to the different inlets/outlets reproduce the actual test-bench operating condition. The effects of the lubricating circuit and of the external environment are represented with a pair of properly defined heat transfer coefficient and reference temperature.

The heat fluxes applied on the boundaries facing the combustion chambers and on the intake and exhaust ports come from in-cylinder simulations, whose setup will be accurately described in the following paragraphs. The thermal loads are point-wise distributions of a cycle-average combustion simulation and they are directly applied to the combustion dome and to the intake and exhaust ports. In order to take into account the revolution of the valves, the heat fluxes are separately space averaged over the faces and the stems. The valves are placed in the closed position and the heat transfer to the seats accounts for the lack of contact during a portion of the engine cycle by means of a contact resistance.

Since the piston is not included in the domain, the point-wise heat flux distribution on the liner is increased adding the contribution of the heat transfer from the piston skirt and rings and the quote of the friction acting on the cylinder due to the piston motion. Such contributions are separately analyzed as described in previous works of the authors [16].

A time-averaged heat flux distribution is imposed on the piston crown. Frictions due to the skirt and to the rings are evaluated based on the in-cylinder pressure trace, and they are split between the piston and the liner. The quote acting on the piston is added to the heat exchanged through the rings, which is mimicked by a pair of thermal resistance and reference temperature derived from [17] and calculated as a resistance network, as depicted in Figure 2 and Figure 3.
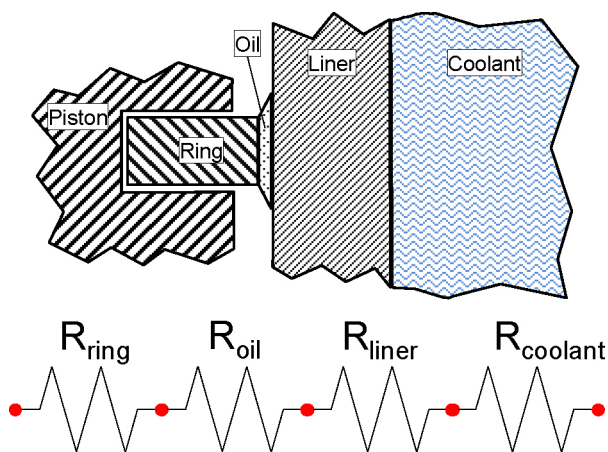
Figure 2. Scheme of the resistance network between the piston groove and the coolant circuit
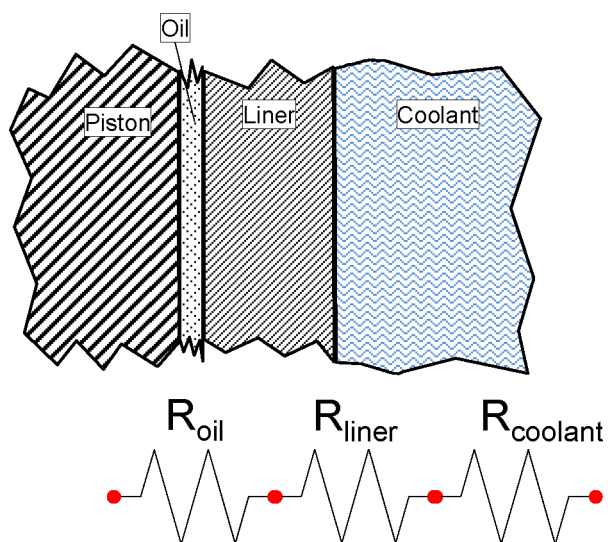

Figure 3. Scheme of the resistance network between the piston skirt and the coolant circuit

The effects on the piston underside are represented with a properly calculated pair of heat transfer coefficient and reference temperature. In particular, to account for the heat removal due to the oil jets acting on the piston underskirt, a heat transfer coefficient distribution similar to that proposed in [18] is applied. In particular, it is modified to consider the relative velocity between the piston and the oil jet, which strongly influences the removed heat amount. Furthermore, the motion of the stagnation point going from TDC to BDC is taken into account. A typical heat transfer coefficient distribution is shown in Figure 4.

A schematic representation of the piston boundary conditions is reported in Figure 5, where all the effects are simultaneously taken into account.

The resulting heat fluxes exiting from the rings and from the skirt are then added to the friction portion and to the combustion loads acting on the cylinder liner. Each contribution due to a complete engine cycle is applied only on the cylinder liner portion affected by it, as depicted in Figure 6, where all the thermal loads acting on the cylinder liner are reported.
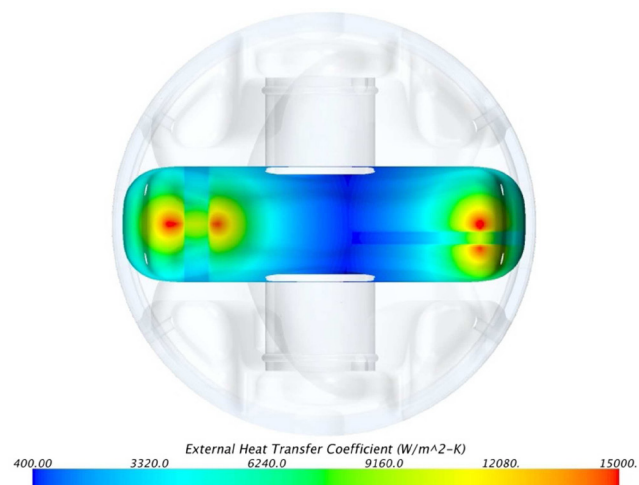

External Heat Transfer Coefficient (W/m^2–K)

400.00   3320.0   6240.0   9160.0   12080.   15000.

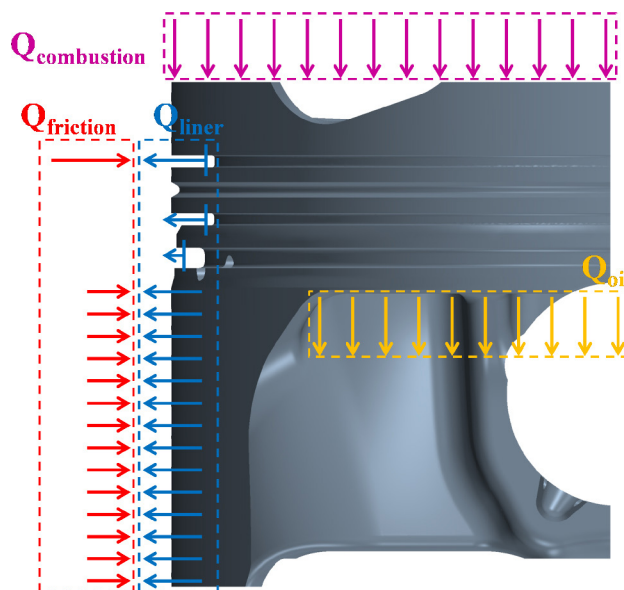Figure 4. Heat transfer distribution on the underskirt portion of the piston

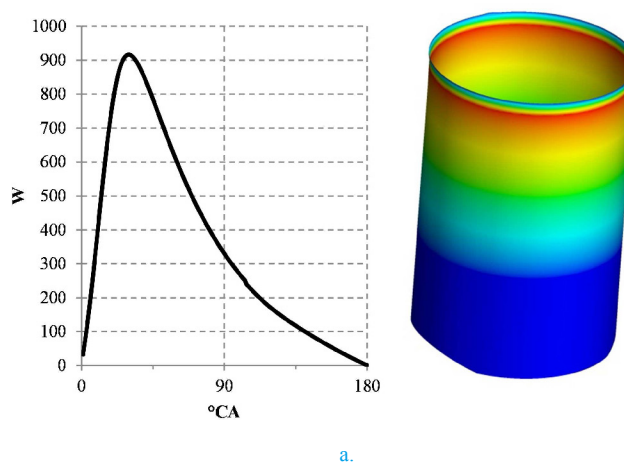Figure 5. Piston thermal boundary conditions

a.

Figure 6. a) Heat flux due to the piston rings friction; b) heat flux due to the piston skirt friction; c) heat transfer from the piston to the liner
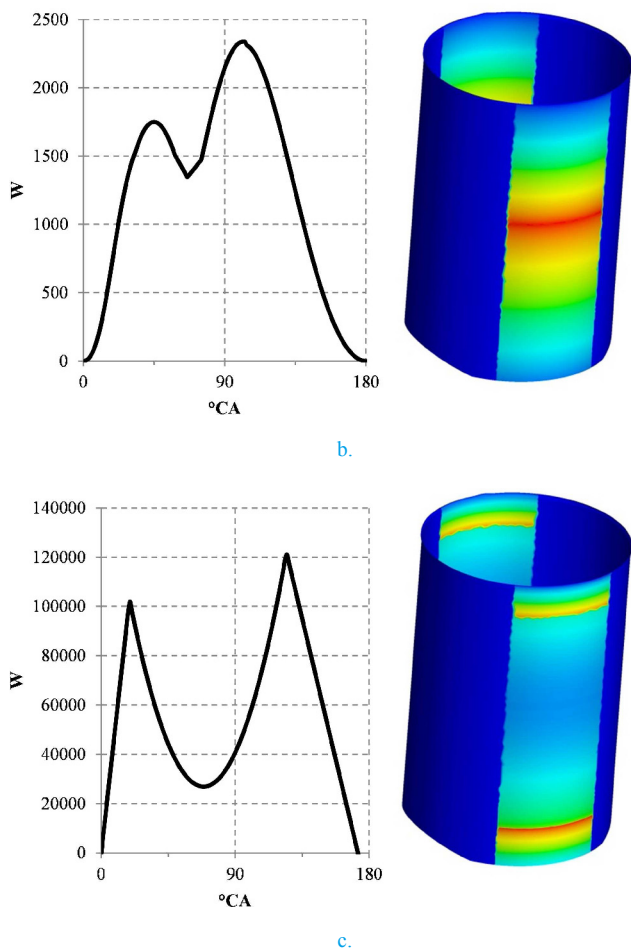
b.

c.

Figure 6. (cont.) a) Heat flux due to the piston rings friction; b) heat flux due to the piston skirt friction; c) heat transfer from the piston to the liner

The resulting thermal load is the sum of all the aforementioned contributions and the cycle-averaged combustion heat fluxes, as schematically depicted in Figure 7.
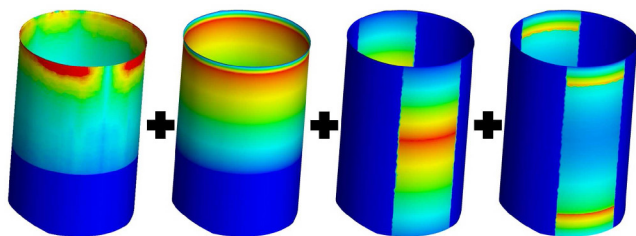

Figure 7. Thermal loads on the cylinder liner. From the left to the right side are reported the heat fluxes due to: the combustion, the piston rings, the piston skirt, the conduction from the piston.

Methodology Limitations

The simulation results for both Engine A and Engine B are compared with experimental temperatures, which are measured by means of several thermocouples placed in the most interesting locations of the engines such as between the exhaust ports, in the peripheral portions of the combustion dome and along the liners in different angular positions, aiming at well capture the engine thermal status.

Calculated temperatures versus experimental ones are depicted in Figures 8, 9, 10 and 11 for all the analyzed operations. The simulated engine thermal field is always over-predicted for both engine head and engine block, and this is due to the overestimation of the wall heat fluxes calculated by the in-cylinder simulations.
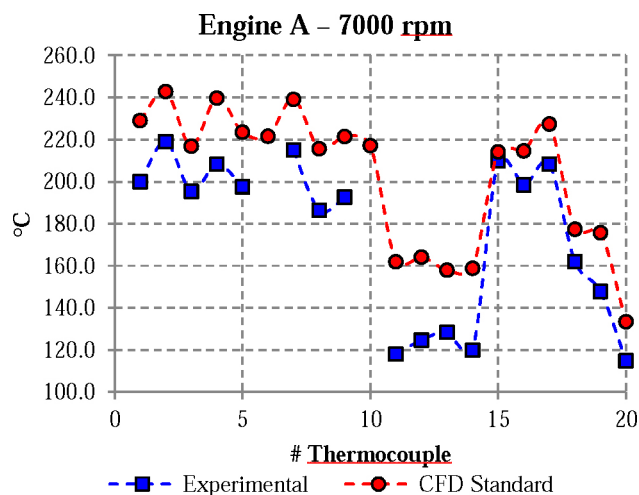

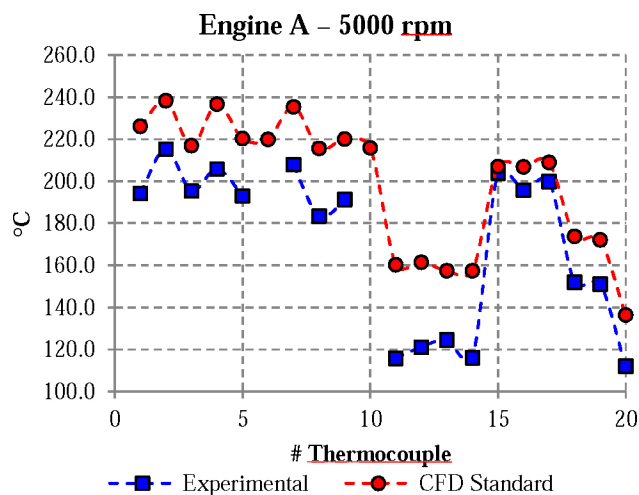Figure 8. Experimental vs numerical temperatures for engine A @ 7000 rpm

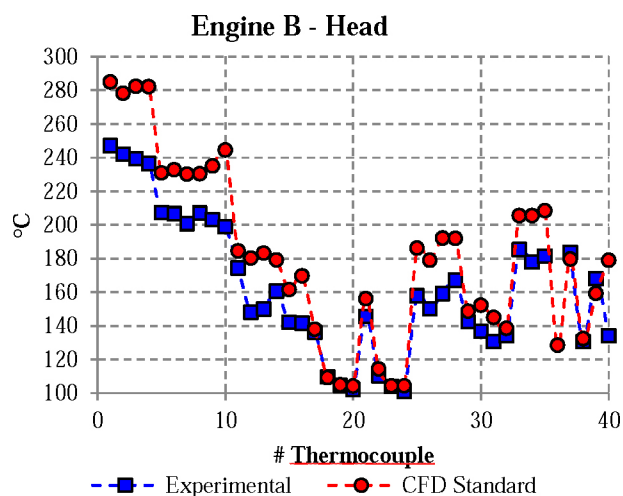Figure 9. Experimental vs numerical temperatures for engine A @ 5000 rpm

Figure 10. Experimental vs numerical temperatures for engine head B
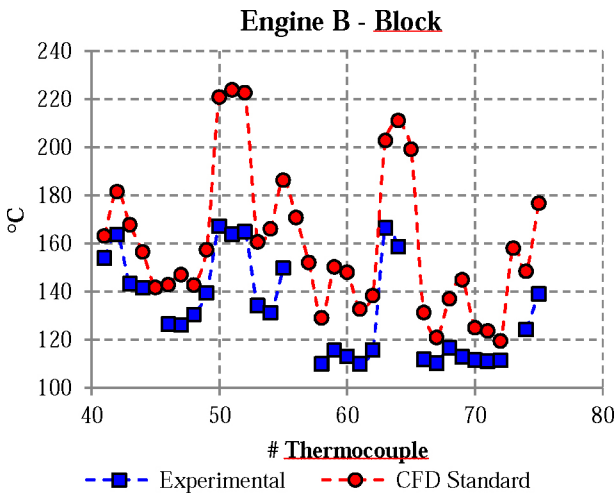
Engine B - Block

Figure 11. Experimental vs numerical temperatures for engine block B

Furthermore, this critical behavior is confirmed by the comparison between the calculated coolant temperature rise and the experimental one. Starting from these evidences the need to critically analyze the thermal wall function formulations adopted for the in-cylinder simulations emerges; in fact, they are the main suspect for the wall heat flux over-prediction. To identify the most suitable thermal law of the wall, the experimental data deriving from the available engine thermal surveys are used, as explained in the following paragraph.

ENGINE THERMAL SURVEY

From a general point of view, an engine at a fixed operation can be analyzed as a steady-state system where energy enters and exits. The chemical energy stored into the fuel is converted into thermal energy (which in turn heats up the lubricating and the coolant circuits and increases the exhaust gas enthalpy) and into indicated work.

The most important role in terms of heat removal is played by the coolant circuit, whose layout for the analyzed engines is schematically reported in Figure 12.
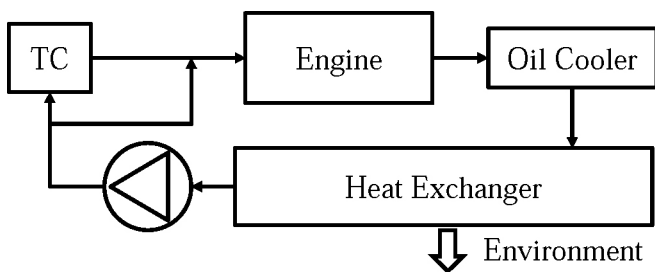

Figure 12. Coolant circuit simplified layout

The coolant surrounds the turbocharger, then enters the engine and finally cools down the lubricating circuit. All the thermal power is then restituted to the environment by means of a heat exchanger.

It is possible to estimate the heat transfer pertaining to each portion of the circuit by placing ad-hoc thermocouples at the inlets and outlets of each element.

In the CHT computational domain just the portion of the coolant circuit represented by the block "engine" in Figure 12 is included Thanks to the many data which are usually collected during the experimental tests it is possible to correctly identify the heat removed by the coolant circuit when it passes through the engine galleries. This amount is almost totally due to the wall heat flux related to the combustion, so it can be used to identify the correct thermal wall function able to evaluate the thermal loads acting on the components facing the combustion chamber.

From the thermal balance reported in Figure 13 it is possible to reconstruct the thermal load acting on the walls due to combustion, as explained in (1):

$$\dot{Q}_{comb} = \dot{Q}_{coolant} + \dot{Q}_{env} + \dot{Q}_{lubr} - \dot{Q}_{fric} - \dot{Q}_{surr}$$
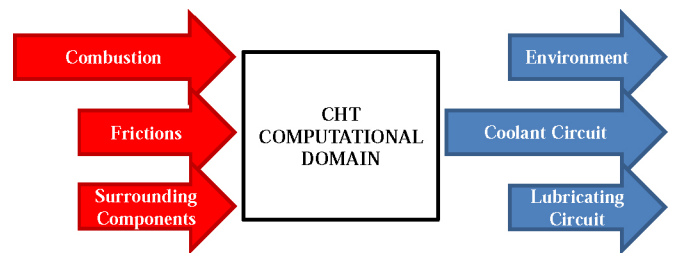
(1)

Figure 13. Engine thermal balance

Only the term $\dot{Q}_{coolant}$ reported in the right side of (1) is strongly affected by a variation of $\dot{Q}_{comb}$ because the coolant circuit surrounds the combustion chamber and removes the largest amount provided to the walls by the combustion. The other terms in (1) can be assumed to be almost constant and can be evaluated from the operating conditions (i.e. the frictions and the heat transfer from surrounding components) or from preliminary CHT simulations (the contribution of the environment and of the lubricating circuit).

The resulting target wall heat fluxes derived from the integration between the data deriving from the thermal survey of each operation and the data deriving from preliminary CHT calculations are reported in Table 3.

Table 3. Engine thermal balance

	Coolant Circuit	Lubricating Circuit	Environment	Surrounding components	Frictions	Combustion Target	Cylinder Target
	kW	kW	kW	kW	kW	kW	kW
Engine A 7000 rpm	114.36	1.20	1.49	4.00	4.38	108.67	13.58
Engine A 5000 rpm	85.68	1.00	1.00	2.00	3.25	82.43	10.30
Engine B	80.20	0.85	2.00	43.90	2.68	36.47	9.12

IN-CYLINDER FRAMEWORK: THERMAL WALL FUNCTION IDENTIFICATION

In-cylinder calculations are performed on the two investigated engines (A and B) to obtain gas-to-wall heat fluxes, whose application in CHT analyses is described above. Experimental data are available for both the engines and they are used to purposely calibrate 1D-CFD models, which in turn provide boundary conditions for the 3D-CFD simulations. Once ignition and combustion models are tuned, the attention is focused on heat fluxes. Two of the most popular heat transfer models used in commercial codes are preliminarily tested. Since a marked overestimation of the heat dissipated at the boundaries is predicted, different formulations are deeply investigated also through the use of one of the most widespread test cases available in literature, i.e. the GM pancake engine. The thermal wall function which represents the best tradeoff for all the engines and operating conditions is presented below together with the results that it provides.

Numerical Setup

The in-cylinder 3D-CFD analyses presented in this paper are carried out by means of a customized version of Star-CD v4.22, licensed by CD-adapco. Time varying pressure and temperature boundary conditions are derived from tuned 1-D model supplied by engine manufacturers. The adopted turbulence model is the k-ε RNG for compressible flows. Both for engine A and B, the computational mesh used in the 3D simulations covers the overall combustion system of one cylinder, including the in-head portions of the intake and exhaust ports; geometrical symmetry was not exploited even if it may be used for engine A. All the simulations are performed in a RANS framework. The total number of fluid cells at TDC is about 700.000 and 500.000 for engine A and B respectively; layer addition and removal is adopted to account for mesh motion, leading to a maximum of 1.5 million and 1 million cells at BDC for the two units. For the high-pressure fuel injection simulation, a pre-atomized population of Lagrangian particles is assigned to each of the injector nozzles of the two engines by means of user coded routines, following the strategy described in [19]. The secondary break-up is modelled by means of the Reitz model [20] while the Bai approach [21] is adopted for droplet wall interaction. The adopted combustion model is the ECFM-3Z [22], which has been widely used in previous publications by the authors [7,9,15-16]. No knock model is used, as the investigated operating points of the two engines are experimentally known as knock-safe. A spatial distribution of temperature, provided by the CHT simulations, is mapped onto the combustion chamber walls and used as boundary condition. Preliminary calculations are run using two heat transfer models available in the Star-CD package and widely adopted in many commercial codes: they are the Angelberger [12] and Han and Reitz [11] laws of the wall respectively. The flame quenching model proposed by Bruneaux [23] is adopted to account for the thermal loss caused by the presence of cooled walls.

First Results

The 3-D CFD models are preliminarily tuned to match the 1-D incylinder average pressure traces. A relatively simple flame kernel deposition model is used and calibrated close to the experimental spark timings (to account for the arc delay); injected fuel, trapped mass, start of injection angle (SOI) and valve lift perfectly match the actual engine operations. Several subsequent engine cycles are performed for each investigated operation in order to reach a fully converged solution. A comparison between 1D-CFD and 3D-CFD curves of in-cylinder pressure is presented in Figure 14.

Once the 3D-CFD simulations are calibrated, the attention is focused on the heat fluxes calculated through the adopted wall heat transfer models. In particular, CHT calculations, described above, clearly highlight a relevant overestimation of the heat losses through the combustion chamber walls predicted by both models. Unfortunately, experimental instantaneous heat fluxes are not available for the investigated engines, since these measurements are far beyond the usual industrial practice and available data in literature are limited to engines and operating conditions far away from the high-speed full-load points. Nevertheless, thanks to the available engine heat rejection thermal balance, the global time-averaged heat flux that is expected to be released by the combustion process to the surrounding walls can be inferred. Under the assumption of homogeneous thermal loss among all the cylinders, a target is found for the time-averaged heat fluxes produced by the in-cylinder 3-D combustion simulations. Figure 15, referred to engine A operating condition 1, shows the numerical instantaneous boundary heat transfer on each combustion chamber component by means of the Angelberger thermal wall of the law (colored dashed lines). The instantaneous total amount is given by the sum of all these contributions and it is represented by the black dashed line. This quantity can be cycle averaged, and it is depicted in Figure 15 with the solid black line. However, only a part of this thermal load is used in the CHT model. As previously explained in the "CHT model and numerical setup" paragraph, the piston is not included in the computational domain, and its contribution to the cylinder liner is just a portion of the heat flux entering the piston crown. This quoted part, summed to the wall heat fluxes acting on all the other boundaries, is represented by the dotted solid black line in Figure 15. This resulting amount can now be compared to the target average heat transfer extrapolated from the experimental thermal balance, previously discussed in the paper, which is represented by the solid crossed black line.

Similarly, Figure 16 shows the previously discussed quantities for the engine A operating condition 1 in the case of the Han and Reitz thermal law of the wall. For the sake of brevity, the operating condition 2 of engine A and the engine B case are not reported, since they show exactly the same trends. As it can be observed from both Figures, both heat transfer models predict a largely overestimated heat flux, whose time-averaged value exceeds by more than 30% the value inferred from the heat rejection analysis. This explains why, as showed in the first section of the paper, the temperatures predicted by the CHT models of both engines are unacceptably higher than the experimentally measured ones.
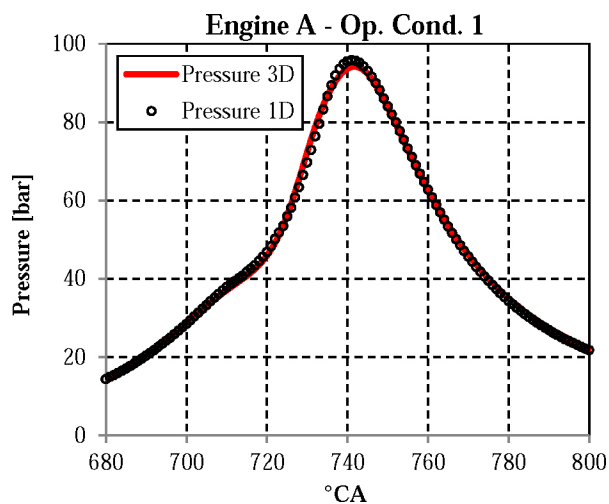
a.
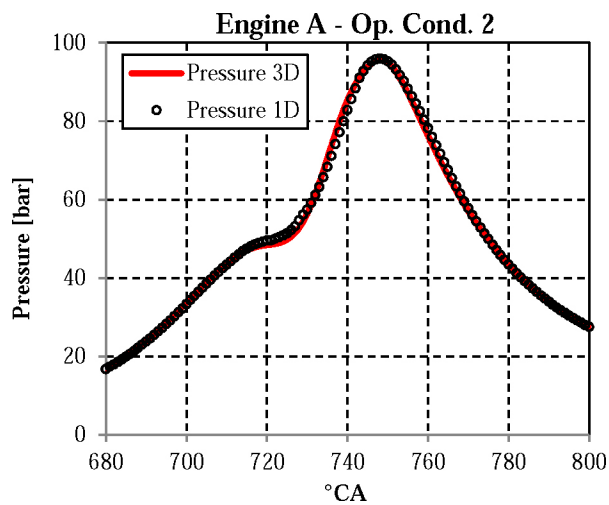
b.
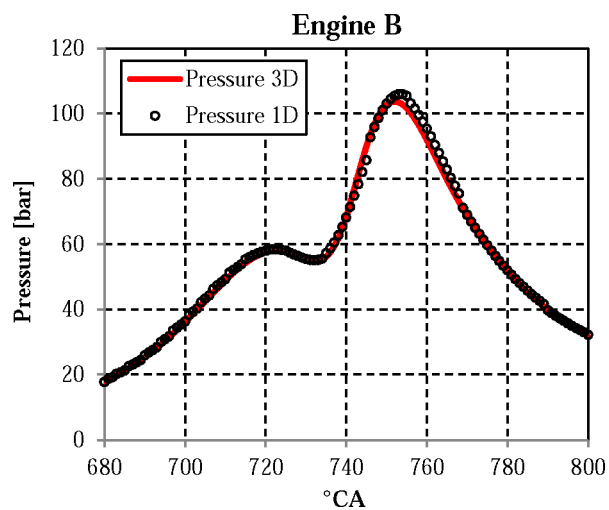
c.

Figure 14. 1D-CFD vs 3D-CFD in-cylinder pressure traces for (a) Engine A Operating condition 1, (b) Engine A Operating condition 2, (c) Engine B
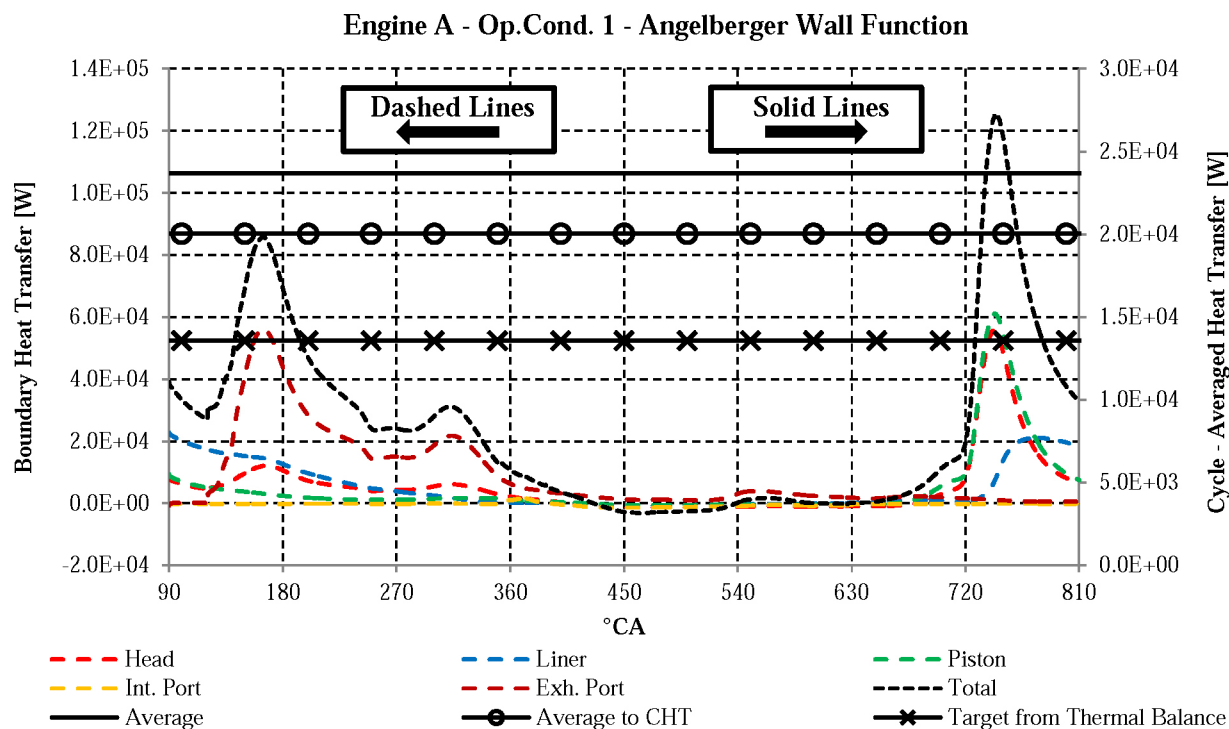
Engine A - Op.Cond. 1 - Angelberger Wall Function

Figure 15. Instantaneous numerical wall heat fluxes (dashed lines) and cycle-averaged heat fluxes (solid lines)

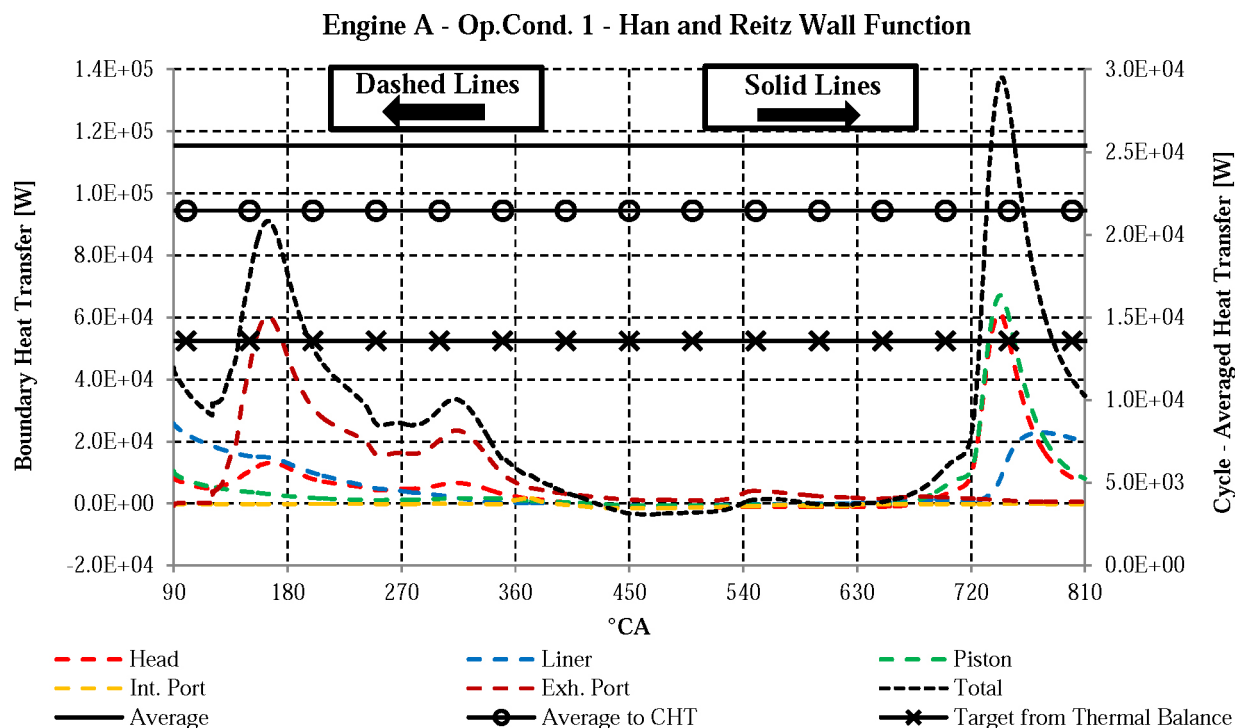**Engine A - Op.Cond. 1 - Han and Reitz Wall Function**

Figure 16. Instantaneous numerical wall heat fluxes (dashed lines) and cycle-averaged heat fluxes (solid lines)

Wall Heat Transfer Model

In order to better understand the rationale of the adopted model, Angelberger and Han and Reitz laws of the wall are briefly recalled. These models are somehow similar both in formulation and in principle: they take into account the variation of density and viscosity

within the boundary layer and are actually a compressible version of the traditional engine wall treatments, in which gas compressibility is not accounted for. Their formulation is reported in (2) and (3).

• Angelberger thermal law of the wall:

$$\begin{cases} \theta^+ = Pr \cdot \eta^+; \ \eta^+ \leq 13.2 \\ \theta^+ = 2.075 \cdot \ln(\eta^+) + 3.9; \ \eta^+ > 13.2 \end{cases}$$

(2)

- Han and Reitz thermal law of the wall:

$$\theta^+ = 2.1 \cdot \ln(\eta^+) + 2.5$$

(3)

For both temperature profiles the wall heat flux formulation is given by (4):

$$q_w = -\frac{\rho_w \cdot c_p \cdot u_\tau \cdot T_w \cdot ln\left(\frac{T}{T_w}\right)}{\theta^+}$$

(4)

where $\eta^+ = (v_w/v) \cdot y^+$ is the non-isothermal dimensionless distance. Strictly speaking, it should be $d\eta^+ = (v_w/v) \cdot dy^+$, but to provide an easier implementation a simplification is introduced to relate η^+ and y^+.

A similar law of the wall was already proposed by Kays and Crawford for isothermal (or incompressible) flow, as reported in (5):

$$T^+ = 2.075 \cdot \ln(y^+) + 13.2 \cdot Pr - 5.34$$

(5)

Limiting considerations to air (for which Prandtl number can be assumed equal to 0.7), it becomes

$$T^+ = 2.075 \cdot \ln(y^+) + 3.9$$

(6)

and the wall heat flux is defined as:

$$q_w = -\frac{\rho_w \cdot c_p \cdot u_\tau \cdot (T - T_w)}{T^+}$$

(7)

Angelberger employs Kays and Crawford formulation to develop its own law of the wall, while Han and Reitz expression slightly differs in order to take into account turbulent Prandtl number variations in the buffer and viscous sublayers. The most relevant difference between Angelberger and Han and Reitz laws of the wall, if compared to Kays and Crawford heat transfer model, is that the dimensionless distance and the dimensionless temperature are redefined so that temperature changes in the near wall region are taken into account. The new dimensionless temperature and distance become:

$$d\eta^+ = (v_w/v) \cdot dy^+ \qquad d\theta^+ = (\rho/\rho_w) \cdot dT^+$$

(8)

Starting from (6) and (7) and adopting the new variables (8), Angelberger heat flux formulation (4) can be obtained.

From a practical point of view, it is not pretentious to say that isothermal laws of the wall are applied to non-isothermal problems simply introducing new variables to redefine dimensionless distance and temperature.

The alternative approach, proposed in this paper and already defined by Angelberger in [24] as "ad-hoc" remedy, is somehow different. Isothermal laws of the wall are applied to non-isothermal problems once again, but unlike the approaches described above where new variables are introduced in order to take into account the compressibility of the gas in the near wall region, new scales of velocity, temperature and wall distance are here introduced for the inner zone of the boundary layer. Compared to Kays and Crawford's heat transfer model, where such scales are computed as:

$$u_\tau = \sqrt{\frac{\tau_w}{\rho_w}} \qquad T_\tau = \frac{q_w}{\rho_w \cdot c_p \cdot u_\tau} \qquad y_\tau = \frac{v_w}{u_\tau}$$

(9)

now the new scales are:

$$u_\tau^* = \sqrt{\frac{\tau_w}{\rho}} \qquad T_\tau^* = \frac{q_w}{\rho \cdot c_p \cdot u_\tau} \qquad y_\tau^* = \frac{v}{u_\tau}$$

(10)

where ρ and v are the mean density and viscosity of the inner zone (values at the centroid of the near wall cell are used). These scales are used to obtain non-dimensional wall distance and temperature respectively:

$$y^{+*} = \frac{y}{y_\tau^*} \qquad T^{+*} = \frac{T - T_w}{T_\tau^*}$$

(11)

The resulting wall heat flux formulation is:

$$q_w = -\frac{\rho \cdot c_p \cdot u_\tau \cdot (T - T_w)}{T^{+*}}$$

(12)

where T^{+*} assumes the following form

$$T^{+*} = 2.075 \cdot \ln(y^{+*}) + 3.9$$

(13)

According to this approach, an isothermal law of the wall can be applied to non-isothermal problems if variables are made dimensionless by means of mean thermodynamic properties (ρ and v) of the inner zone rather than wall properties (ρ_w and v_w). Even if pretty physical, this approach cannot be justified through a rigorous mathematical demonstration starting from such simplified equations of the inner zone of the boundary layer with variable thermodynamics properties.

The proposed heat transfer model is then slightly modified by the authors in order to account for Prandtl number variations. As a consequence, unlike expression (13) T^{+*} assumes its original form:

$$T^{+*} = 2.075 \cdot \ln(y^{+*}) + 13.2 \cdot Pr^* - 5.34$$

(14)

in which $Pr^* = \mu \cdot c_p/\lambda$ is the Pr number and the star evidences its possibility to vary, if compared to (5).

In fact, unlike Kays and Crawford which assume constant Pr in space (i.e. in the viscous sublayer along the normal direction to the wall, necessary assumption for the integration of the simplified energy equation) and time, as depicted above through equations (5) and (6), Pr is here constant in space but not in time. It is recomputed every time step for each near wall cell according to specific heat, thermal conductivity and dynamic viscosity evaluated on the local temperature.

Therefore, the thermal law of the wall proposed by the authors in (14) differs from the Kays and Crawford one (5) for two main characteristics: the non-dimensional distance is computed thanks to the new scales and the Pr number is no more constant but it can vary following the local and instantaneous condition.

Before applying the proposed approach, hereafter referred to as "Modified", to the investigated engines, some considerations can be drawn for the GM pancake test case. As known, this engine is a SI engine with a central mounted spark, fueled with propane, whose main geometrical characteristics are reported in table 3. Local wall heat flux measurements are available thanks to the experimental investigation performed by Alkidas [5] and Alkidas and Meyers [6]. The simulation starts at 117°CA bFTDC (which corresponds to IVC) and ends at 80°CA aFTDC. As in previous studies available in literature, the gas exchange is not modeled. This leads to an axisymmetric pancake geometry of the simulation domain. Initial and boundary conditions are widely discussed in [24,25] and briefly reported in table 4 together with the investigated operating conditions reported in table 5.

Table 3. Pancake engine geometrical data

Bore	105 [mm]
Stroke	95.25 [mm]
Connecting Rod Length	158 [mm]
Compression Ratio	8.56

Table 4. Initial and boundary conditions

TKE (k)	84 [m²/s²]
Length scale (L)	0.93 [cm]
Pressure	0.821 [bar]
Temperature	449 [K]
Mass Composition	Y_{C3H8}=4.6 % Y_{O2}=18.76 % Y_{N2}=73.7 % Y_{CO2}=1.89 % Y_{H2O}=1.04 %
Wall Temperatures	T_{Head}=445 K T_{Liner}=405 K T_{Piston}=445 K

Table 5. Investigated operating conditions

Engine Speed	1500 [rpm]
Equivalence Ratio	0.87
Volumetric Efficiency	40 %
Spark Timing	27° CA bFTDC

As for the velocity field initialization, a linearly decreasing profile from the piston to the cylinder head is imposed. Swirl ratio is assumed to be null.

The adopted mesh contains almost 700.000 cells at 117°CA bFTDC and about 300.000 cells at TDC, with a constant near wall layer size of 1 mm. The combustion model (ECFM-3Z) as well as ignition one are purposely calibrated thanks to the available experimental cylinder pressure trace, and the CFD results are reported in figure 17.
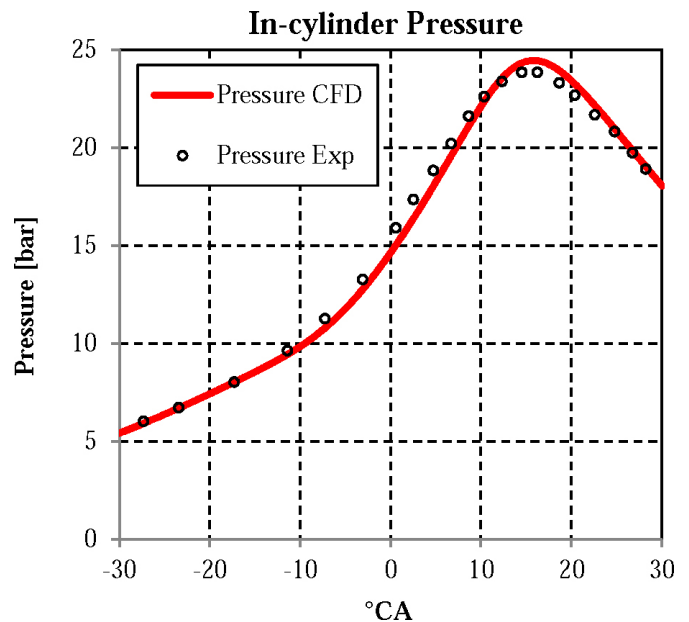

Figure 17. Experimental in-cylinder pressure trace for the Pancake engine and CFD calibration

Once the simulations are calibrated, a comparison between the described heat transfer models is performed. Local wall heat flux measurements are experimentally available thanks to four probes located on the cylinder head (here referred to as HT1 to HT4) and one on the liner (referred to as HT5). The distances of the heat flux probes HT1, HT2, HT3 and HT4 from the spark plug are 18.7, 27.5, 37.3 and 46.3 mm, respectively. HT5 is located 6.3 mm below the head. For sake of brevity just HT1 will be examined, since the remaining probes show very similar trends. Figures 18 and 19 show the values of y^{+*} and wall heat flux at HT1 respectively throughout the simulation.
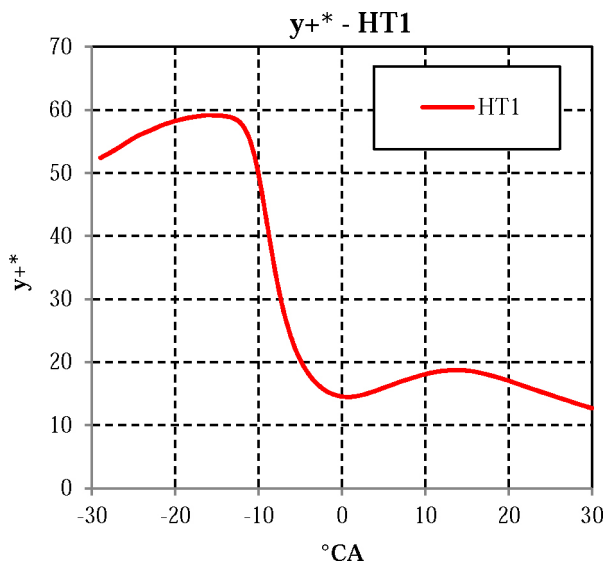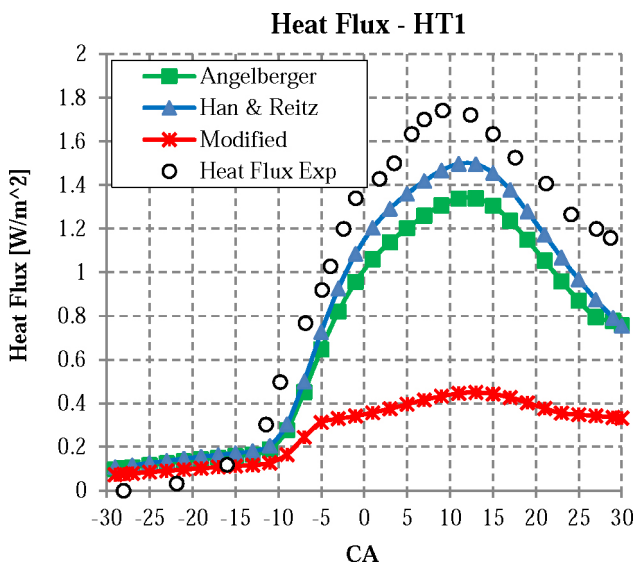
Figure 18. Wall y+* for the in-cylinder simulations.

Figure 19. Heat flux on the HT1: comparison between the experimental data and the numerical simulations

In particular, three different heat transfer models are compared: Angelberger, Han and Reitz and the "Modified" approach proposed in this paper. Given the y^{+*} value, and according to Angelberger formulation, the near wall cell falls in the inertial sublayer, where a logarithmic law of the wall is adopted. Such law differs from the Han and Reitz just for the value of the constant term, which is slightly higher in Angelberger's formulation. As a consequence, the heat flux predicted by the Han and Reitz model is slightly higher than that of Angelberger's model. Despite such difference, both models closely resemble the measured heat flux. As for the proposed formulation, its application to the pancake engine seems to relevantly underestimate the heat transfer from the gases to the walls. Although such deficiency seems to be a promising remedy for the previously outlined strong overestimation under actual highly charged engine conditions, it is interesting to try to understand the origin of such schizophrenic behavior. To this aim, the so-called "isothermicity parameter" ζ can be introduced. Such parameter is defined as:

$$\zeta = \frac{-T_\tau}{T_W} = \frac{-q_w}{\rho_w \cdot c_p \cdot u_\tau \cdot T_w}$$

$$(15)$$

and it can be considered either as a characteristic scale of the ratio between the gas temperature and the wall temperature and as a characteristic scale of the heat flux (it is, in the end, a non-dimensional flux). This implies that whenever ζ asymptotically tends to zero, the heat flux becomes negligible and the gas temperature approaches the wall temperature. In other words, the boundary layer becomes quasi-isothermal and both viscosity and density are nearly constant. Under such conditions, classical formulations for the law of the wall can be adopted. Viceversa, if ζ becomes non-negligible, then the heat flux behaves similarly and temperature, density and viscosity cannot be considered anymore constant within the boundary layer: this is a case of non-isothermal flow, for which models such as the Angelberger and the Han and Reitz were purposely developed and successfully applied. In order to understand why such models correctly match the measurements under the test case conditions and fail for the investigated production engines, the evolution of the ζ parameter on the flame deck, the liner and the piston is reported for both the GM pancake and the highly charged engines. In particular, the ζ value is computed using, for all the cases, a unique heat transfer model, i.e. that proposed by Angelberger, as reported in Figure 20.
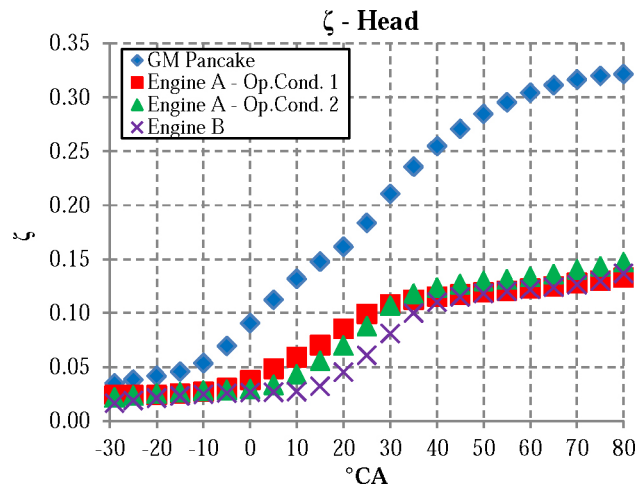
a.
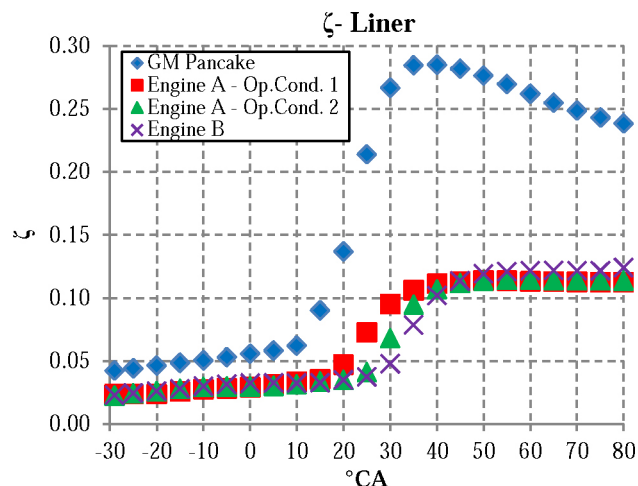
b.

Figure 20. ζ on the head (a), liner (b) and piston (c) of both the GM pancake engine and the investigated engines
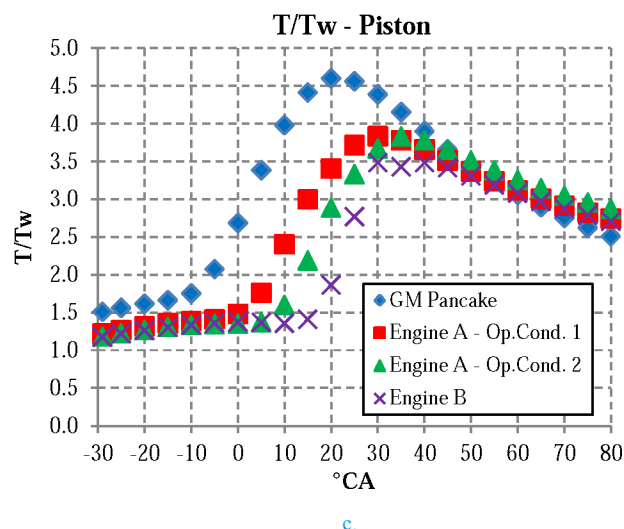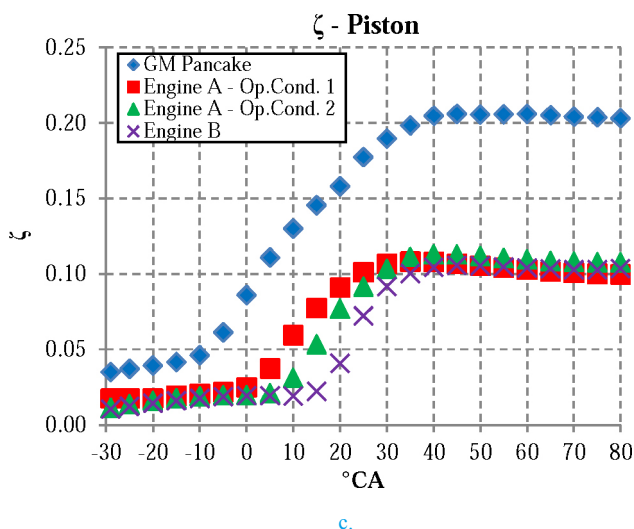
Figure 20. (cont.) ζ on the head (a), liner (b) and piston (c) of both the GM pancake engine and the investigated engines

Figure 21. (cont.) T/Tw ratio on head (a), liner (b) and piston (c) of both the GM pancake engine and the investigated engines
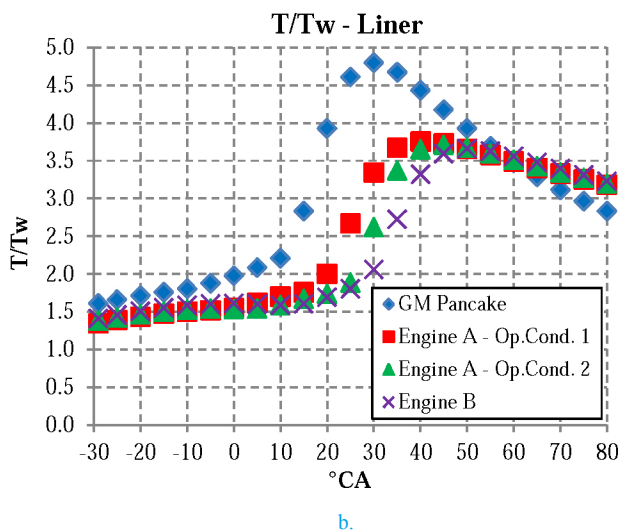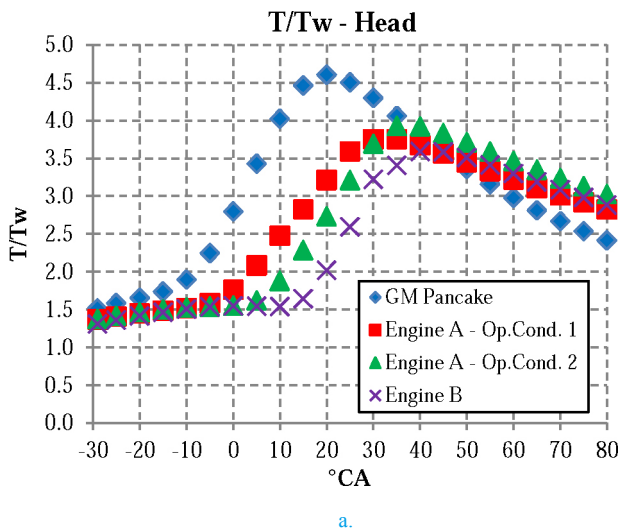

Figure 21.

As visible, for a given wall function the value of ζ in the pancake engine is always much higher than that for the production engines. If we consider such parameter as a characteristic scale of the heat flux and we scale all the quantities by using the overall energy available to the fluid, we can conclude that the investigated engines are characterized by much lower heat flux percentages. The lower ζ values are not to be attributed to "quasi-isothermal" or "more isothermal" boundary layers for the production engines (as visible in Figure 21) since the ratio of gas to wall temperature is almost coincident for all the investigated engines. Such lower values are a consequence of the average in-cylinder pressure level. In fact, under the assumption of ideal gas, we can re-write ζ as follows in eq. 16:

$$\zeta = \frac{-q_w}{p \cdot u_\tau . \gamma / (\gamma - 1)}$$

(16)

being p the in-cylinder pressure and γ the ratio of specific heats.

Despite the production engines are characterized by higher heat fluxes, ζ is lower because of the much higher in-cylinder pressure and turbulence levels. Assuming equal γ for all the engines, both pressure and friction velocity are much higher for the production engines, which are characterized by much higher power densities through engine boosting and high peak revving speeds and high tumble ratios, that lead to maximize in-cylinder turbulent kinetic energy and therefore friction velocity (under the assumption of equilibrium in the inertial sublayer).

To conclude, it is possible to say that despite the relevant heat fluxes, much higher than those of the pancake engine, the investigated production engines exchange less energy through the combustion chamber walls and are therefore characterized by lower ζ values. This brings us to conclude that well-consolidated heat transfer models such as those proposed by Angelberger or Hand and Reitz are capable to correctly predict gas-to-wall heat fluxes for high ζ values, as in the pancake case, while they tend to overestimate fluxes for low ζ values,

i.e. for more "isothermal" engines or engine operations, where the proposed approach shows better consistency with the available experimental information.

Hereafter, such "Modified" wall heat transfer model is then applied to the investigated production engines. As visible, the re-computed heat fluxes are much lower than those previously commented, and the

gas-to-wall heat flux is much closer to the target value to meet the proper engine heat rejection balance, as depicted in Figures 22 to 24.

Such fluxes are therefore used as thermal boundary conditions in a new set of CHT simulations which is described in the following section.
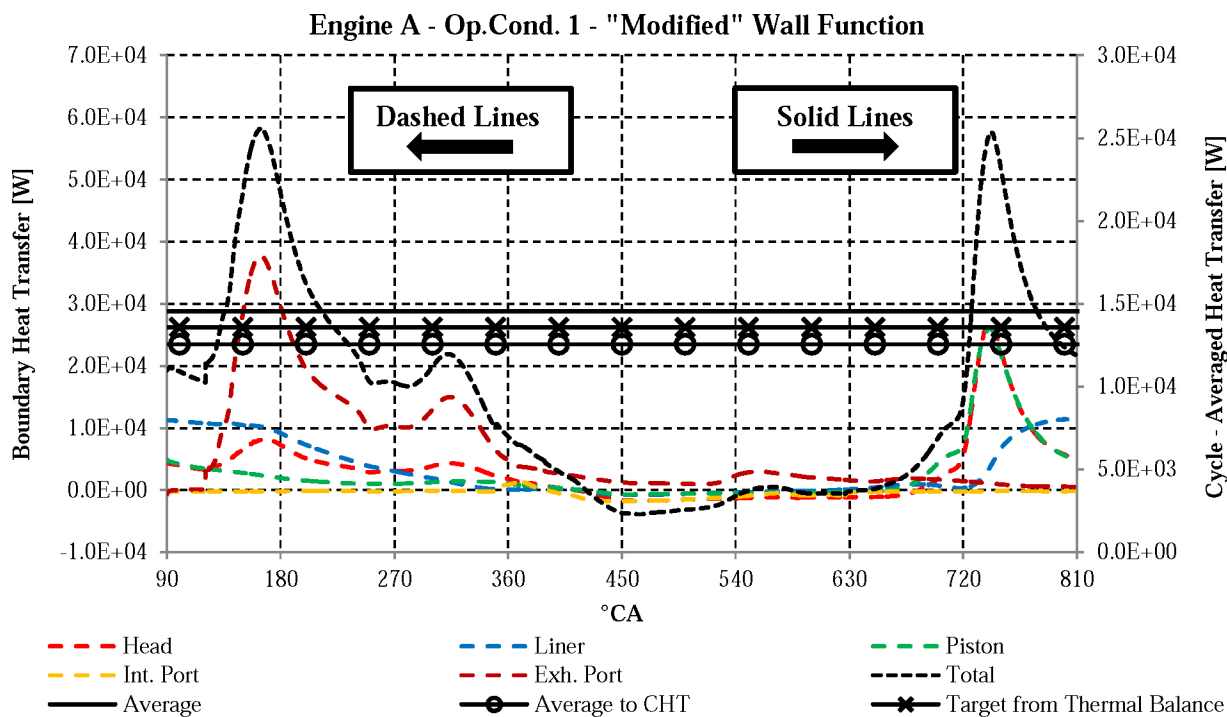

Figure 22. Heat fluxes of engine A operating condition 1 resulting from the "Modified" law of the wall
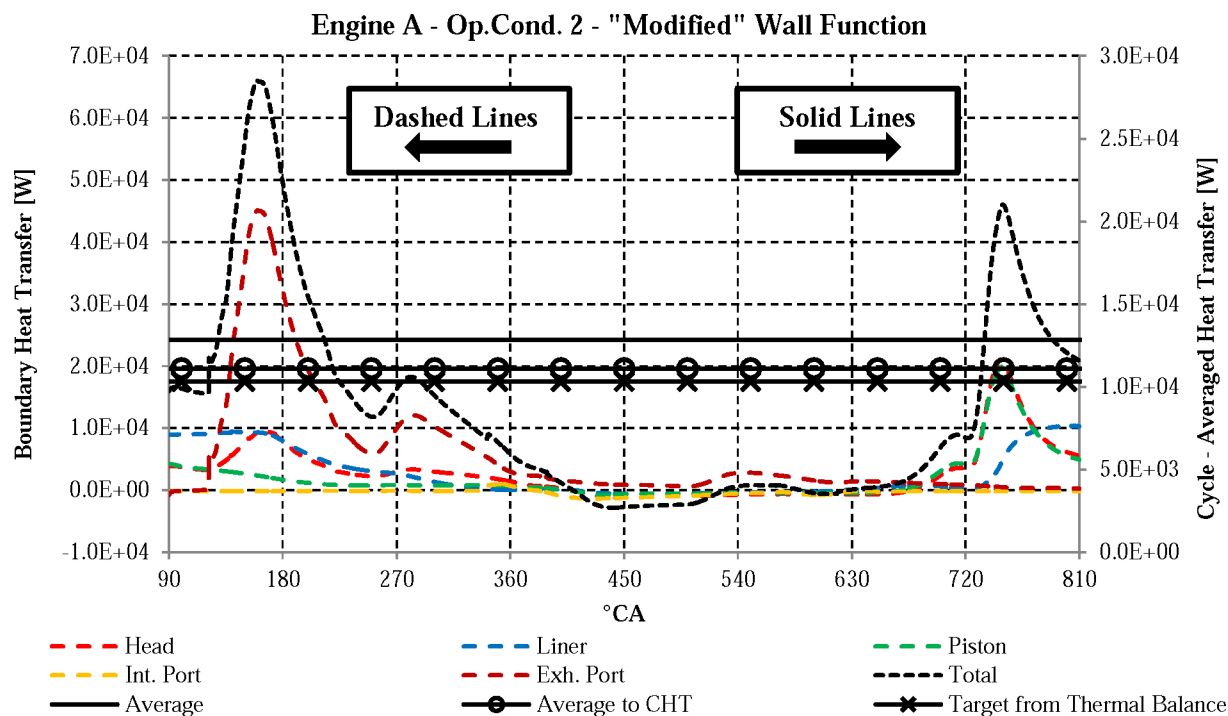

Figure 23. Heat fluxes of engine A operating condition 2 resulting from the "Modified" law of the wall
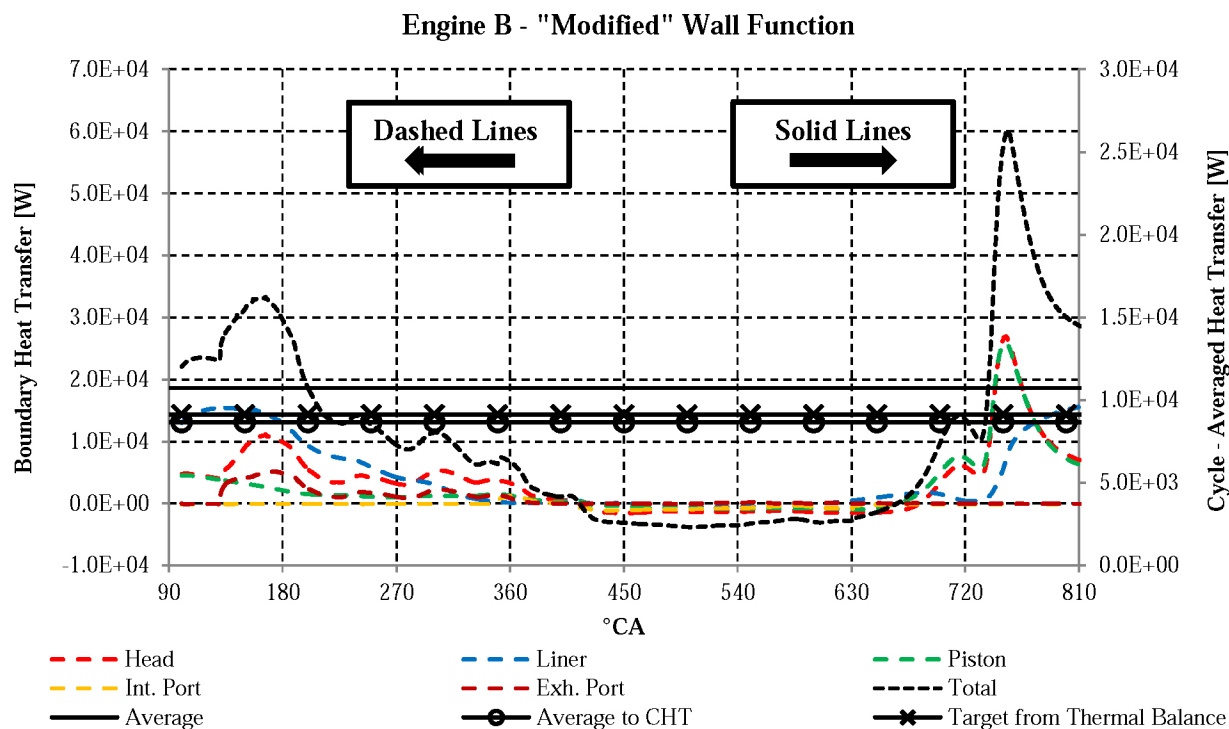
Engine B - "Modified" Wall Function

Figure 24. Heat fluxes of engine B resulting from the "Modified" law of the wall

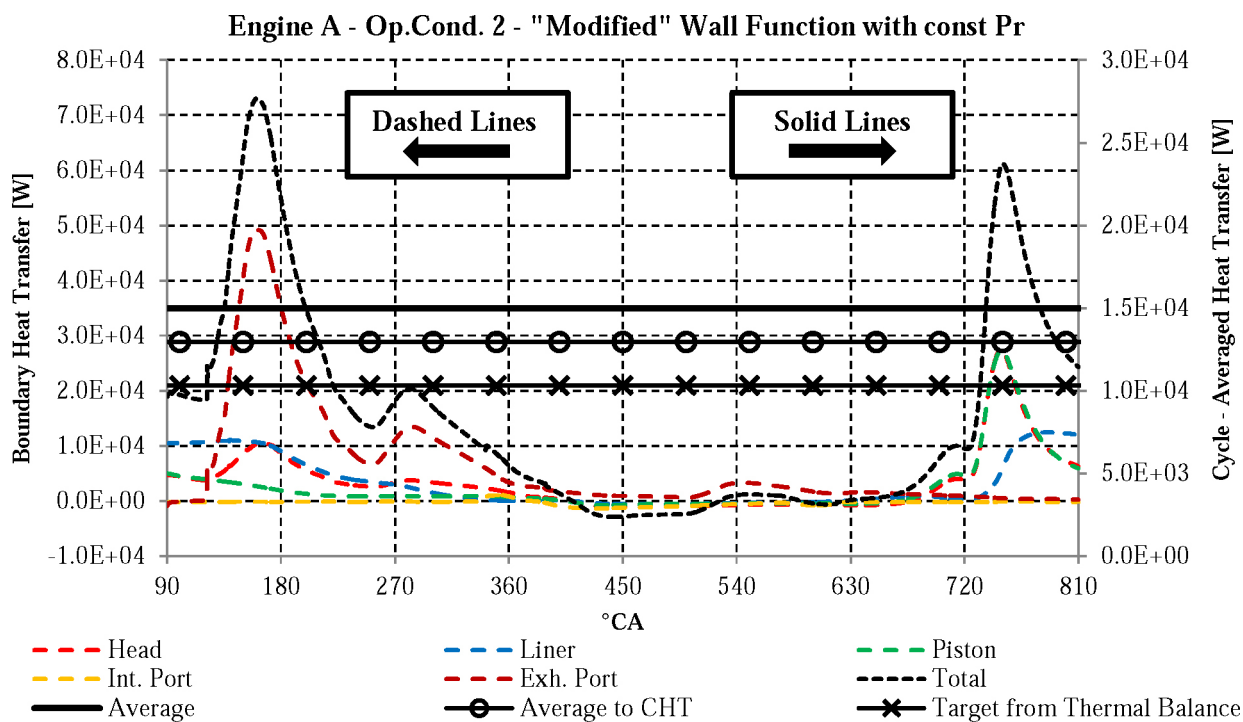**Engine A - Op.Cond. 2 - "Modified" Wall Function with const Pr**

Figure 25. Heat fluxes of engine A operating condition 2 resulting from the "Modified" law of the wall with constant Pr

In order to underline the importance of having a variable Pr number, for engine A operating condition 2 gas-to-wall heat fluxes calculated by means equation (13) are presented in Figure 25. Compared to Figure 23 where the thermal load is computed through equation (14), i.e. a formulation characterized by a variable Pr number, in Figure 25 this latter is kept constant and heat fluxes are higher and further from the target value.

IMPROVED CHT RESULTS

The combustion heat fluxes calculated by means of the "Modified" thermal law of the wall are newly mapped into the CHT model to recompute the engine thermal field. The comparison between the numerical and experimental data is reported in Figures 26 to 29. A very good agreement is achieved and, as a consequence of the methodology, the engine thermal balance is perfectly satisfied.

CONCLUSIONS

A correct evaluation of the engine thermal field requires a proper estimate of the combustion heat fluxes acting on the components facing the combustion chamber. The paper focuses on the predictive capability of some well-known thermal law of the walls commonly available in CFD commercial codes. Such correlations prove to behave correctly when applied to a widely investigated engine test case, while they show some deficiencies when used for the thermal estimation of highly-charged / highly-downsized engines, due to the very different levels of in-cylinder turbulence, pressure and thermal loads. The overestimation of the wall heat fluxes calculated by the commonly used thermal law of the walls is indirectly proved thanks to engine thermal balances and a wide set of experimental temperature measurements of the two engines.

In order to overcome such deficiency, a different approach is proposed and deeply investigated. The new formulation is able to well match both the global engine thermal survey and the local temperature field, and it can be used as a valid predictive tool for high load DISI turbocharged engines.
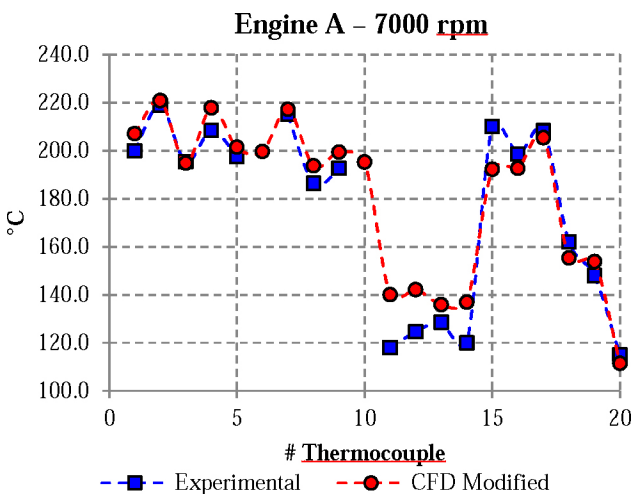

Figure 26. Numerical vs experimental temperature for Engine A @ 7000 rpm
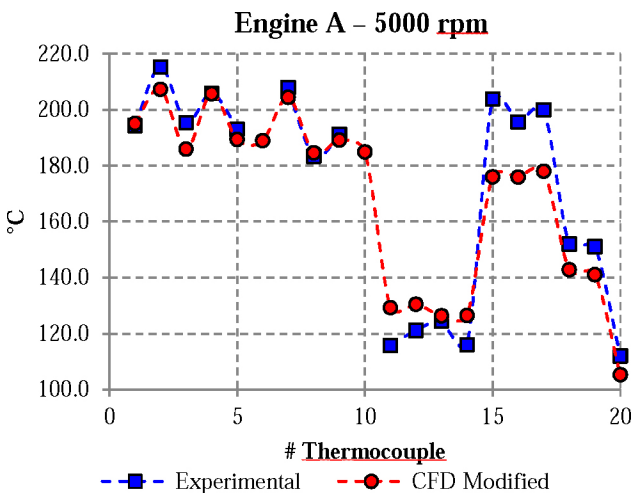

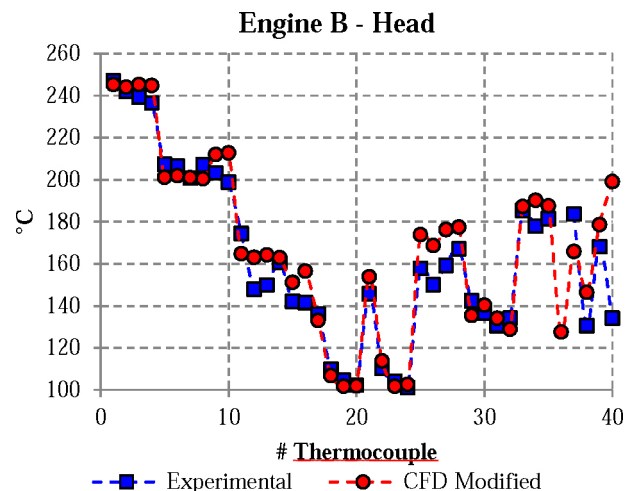Figure 27. Numerical vs experimental temperature for Engine A @ 5000 rpm

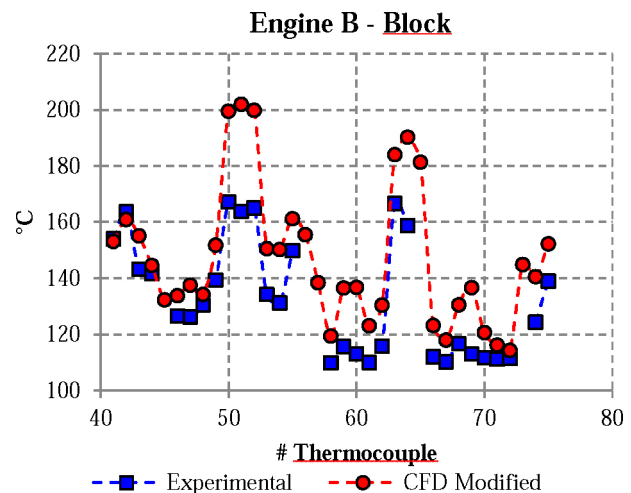Figure 28. Numerical vs experimental temperature for Engine B head

Figure 29. Numerical vs experimental temperature for Engine B block

REFERENCES

1. Turner, J.W.G., Pearson, R.J., and Kenchington, S.A. "Concepts for improved fuel economy from gasoline engines," International Journal of Engine Research; January 1, 2005, vol. 6, 2, pp. 137-157. 4.

2. Fraser, N., Blaxill, H., Lumsden, G., and Bassett, M., "Challenges for Increased Efficiency through Gasoline Engine Downsizing," *SAE Int. J. Engines* 2(1):991-1008, 2009, doi:10.4271/2009-01-1053.

3. Fontanesi, S., d'Adamo, A., Rutland, C.J., "Large-Eddy simulation analysis of spark configuration effect on cycle-tocycle variability of combustion and knock," International Journal of Engine Research, April 2015; Vol. 16, 3: pp. 403-418., first published on January 9, 2015.

4. Fontanesi, S., and Giacopini, M., "Multiphase CFD-CHT optimization of the cooling jacket and FEM analysis of the engine head of a V6 diesel engine," Applied Thermal Engineering; Volume 52, Issue 2, 15 April 2013, Pages 293-303, ISSN 1359-4311, 10.1016/j. applthermaleng.2012.12.005.

5. Alkidas, A.C. "Heat Transfer Characteristics of a Spark-Ignition Engine," ASME. J. Heat Transfer. 1980;102(2):189-193. Doi:10.1115/1.3244258.

6. Alkidas, A.C., Myers, J.P. "Transient Heat-Flux Measurements in the Combustion Chamber of a Spark-Ignition Engine," ASME. J. Heat Transfer. 1982;104(1):62-67. Doi:10.1115/1.3245069.

7. Fontanesi, S., Cicalese, G., Cantore, G., and D'Adamo, A., "Integrated In-Cylinder/CHT Analysis for the Prediction of Abnormal Combustion Occurrence in Gasoline Engines," SAE Technical Paper 2014-01-1151, 2014, doi:10.4271/2014-01-1151.

8. Fontanesi, S., Giacopini, M., Cicalese, G., Sissa, S., Fantoni, S. "Numerical investigation of the cavitation damage in the wet cylinder liner of a high performance motorbike engine," Engineering Failure Analysis, Volume 44, September 2014, Pages 408-423, ISSN 1350-6307, http://dx.doi.org/10.1016/j.engfailanal.2014.05.025.

9. Fontanesi, S., Cicalese, G., d'Adamo, A., Cantore, G. "A Methodology to Improve Knock Tendency Prediction in High Performance Engines," ENERGY PROCEDIA, volume n. 45, pp. 769-778, ISSN: 1876-6102

10. Fontanesi, S., Cicalese, G., and Giacopini, M., "Multiphase CFD-CHT Analysis and Optimization of the Cooling Jacket in a V6 Diesel Engine," SAE Technical Paper 2010-01-2096, 2010, doi:10.4271/2010-01-2096.

11. Han, Z.; Reitz, R.D., "A Temperature Wall Function Formulation for Variable Density Turbulent Flows with Application to Engine Convective Heat Transfer Modeling," International Journal of Heat and Mass Transfer, Vol. 40, No. 3, pp. 613-625, 1997

12. Angelberger, C., Poinsot, T., and Delhay, B., "Improving Near-Wall Combustion and Wall Heat Transfer Modeling in SI Engine Computations," SAE Technical Paper 972881, 1997, doi:10.4271/972881.

13. Rakopoulos, C. D., Kosmadakis, G. M., Pariotis, E. G. "Critical evaluation of current heat transfer models used in CFD incylinder engine simulations and establishment of a comprehensive wall-function formulation,", Applied Energy, 87, 2010, 1612-1630

14. Kays, W.M., Crawford, M. E. "Convective heat and mass transfer," McGraw-Hill, New York, 3rd edition, 1994

15. Fontanesi, S., Cicalese, G., and Tiberi, A., "Combined Incylinder / CHT Analyses for the Accurate Estimation of the Thermal Flow Field of a High Performance Engine for Sport Car Applications," SAE Technical Paper 2013-01-1088, 2013, doi:10.4271/2013-01-1088.

16. Giovannoni, N., d'Adamo, A., Cicalese, G., and Cantore, G., "Effects of Fuel-Induced Piston-Cooling and Fuel Formulation on the Formation of Fuel Deposits and Mixture Stratification in a GDI Engine," SAE Technical Paper 2015-01-0394, 2015, doi:10.4271/2015-01-0394.

17. Esfahanian, V., Javaheri, A., Ghaffarpour, M. "Thermal analysis of an SI engine piston using different combustion boundary condition treatments," Applied Thermal Engineering, Volume 26, Issues 2-3, February 2006, Pages 277-287, ISSN 1359-4311, http://dx.doi.org/10.1016/j.applthermaleng.2005.05.002.

18. Stevens, J.J., Webb, B.W. "Local Heat Transfer Coefficients Under an Axisymmetric, Single-Phase Liquid Jet," ASME. J. Heat Transfer. 1991;113(1):71-78, doi:10.1115/1.2910554.

19. Malaguti, S., Fontanesi, S., Cantore, G., Montanaro, A., Allocca, L., "Modelling of Primary Breakup Process of a Gasoline Direct Engine Multi-Hole Spray," Atomization and Sprays, 23 (10): 861-888 (2013), ISSN Print: 1045-5110, ISSN Online: 1936-2684, 10.1615/AtomizSpr.2013005867

20. Reitz, R. and Diwakar, R., "Effect of Drop Breakup on Fuel Sprays," SAE Technical Paper 860469, 1986, doi:10.4271/860469.

21. Bai, C. and Gosman, A., "Mathematical Modelling of Wall Films Formed by Impinging Sprays," SAE Technical Paper 960626, 1996, doi:10.4271/960626.

22. Colin, O., Benkenida, A., "The 3-Zones Extended Coherent Flame Model (ECFM3Z) for Computing Premixed/Diffusion Combustion," Oil & Gas Science and Technology - Rev. IFP, Vol. 59 (2004), No. 6, pp. 593-609

23. Bruneaux, G., Poinsot, T., Ferziger, J.H. "Premixed flame-wall interaction in a turbulent channel flow: budget for the flame surface density evolution equation and modelling," Journal of Fluid Mechanics, 349, pp 191-219 doi:10.1017/S0022112097006769

24. Angelberger, C. "Contributions à la modélisation de l'interaction 17lame-paroi et des flux pariétaux dans les moteurs à allumage commandé," PhD Thesis, 1997

25. Saric, S. and Basara, B., "A Hybrid Wall Heat Transfer Model for IC Engine Simulations," *SAE Int. J. Engines* 8(2):411-418, 2015, doi:10.4271/2015-01-0388.

DEFINITIONS/ABBREVIATIONS

B - Bore

S - Stroke

BMEP - Brake Mean Effective Pressure

°CA - Crank Angle Degree

aFTDC - After Firing Top Dead Center

bFTDC - Before Firing Top Dead Center

θ^+, T^{+*} - Non-isothermal dimensionless temperature (i.e. dimensionless temperature for non-isothermal boundary layer)

η^+, y^{+*} - Non-isothermal dimensionless distance (i.e. dimensionless distance for non-isothermal boundary layer)

q_w - Wall heat flux

ρ - Density

ρ_w - Density at the wall

C_p - Specific heat at constant pressure

u_τ, u_τ^* - Friction velocity

T - Temperature

T_w - Wall temperature

T_τ, T_τ^* - Characteristic temperature of the inner layer

T^+ - Dimensionless temperature

y_τ, y_τ^* - Characteristic length of the inner layer

y^+ - Dimensionless distance

ν - Kinematic viscosity

ν_w - Kinematic viscosity at the wall

μ - Dynamic viscosity

λ - Thermal conductivity

Pr, Pr^* - Prandtl number

ζ - Isothermicity parameter

TKE (k) - Turbulent kinetic energy

p - Pressure

γ - Ratio of specific heats